

Supplementary Material for: "Optical phase mining by adjustable spatial differentiator"

Tengfeng Zhu^a, Junyi Huang^a, Zhichao Ruan^{a,b,*}

^aInterdisciplinary Center for Quantum Information, State Key Laboratory of Modern Optical Instrumentation, and Zhejiang Province Key Laboratory of Quantum Technology and Device, Department of Physics, Zhejiang University, Hangzhou 310027, China.

^bCollege of Optical Science and Engineering, Zhejiang University, Hangzhou 310027, China

*Zhichao Ruan, zhichao@zju.edu.cn

1 Calculation of the spatial spectral transfer function during a reflection process

To calculate the spatial spectral transfer function, we first consider a plane wave with a wavevector \vec{k} between the incident electric field \vec{E}_i and the reflected one \vec{E}_r on the dielectric interface. We define the s- and p-polarizations as the electric field vectors along $\vec{u}_s = \vec{u}_k \times \vec{n} / |\vec{u}_k \times \vec{n}|$ and $\vec{u}_p = \vec{u}_s \times \vec{u}_k$, respectively. Here $\vec{u}_k = \vec{k} / |\vec{k}|$ is the normalized wavevector and \vec{n} is the unit normal vector of the interface. Then, the left- and right-handed circular polarization bases \vec{u}_+ and \vec{u}_- for plane waves are defined as

$$\vec{u}_{\pm} = \frac{1}{\sqrt{2}} (\vec{u}_p \pm i\vec{u}_s). \quad (\text{S1})$$

We can decompose the vectorial fields \vec{E}_i and \vec{E}_r into left- and right-handed circularly polarized plane waves through the spatial Fourier transform:

$$\begin{aligned} \vec{E}_i &= \vec{u}_+^{i0} E_+^{i0}(x, y) + \vec{u}_-^{i0} E_-^{i0}(x, y) + \vec{u}_z^{i0} E_z^{i0}(x, y) \\ &= \iint \left[\vec{u}_+^{i0} \tilde{E}_+^{i0}(k_x, k_y) + \vec{u}_-^{i0} \tilde{E}_-^{i0}(k_x, k_y) + \vec{u}_z^{i0} \tilde{E}_z^{i0}(k_x, k_y) \right] e^{ik_x x} e^{ik_y y} dk_x dk_y, \end{aligned} \quad (\text{S2a})$$

$$\begin{aligned}
\vec{E}_r &= \vec{u}_+^{r0} E_+^{r0}(x, y) + \vec{u}_-^{r0} E_-^{r0}(x, y) + \vec{u}_z^{r0} E_z^{r0}(x, y) \\
&= \iint \left[\vec{u}_+^{r0} \tilde{E}_+^{r0}(k_x, k_y) + \vec{u}_-^{r0} \tilde{E}_-^{r0}(k_x, k_y) + \vec{u}_z^{r0} \tilde{E}_z^{r0}(k_x, k_y) \right] e^{ik_x x} e^{ik_y y} dk_x dk_y.
\end{aligned} \tag{S2b}$$

Here, x and y are the beam coordinates as shown in Fig. 1 in the main text, while z is along the propagation direction of the beam and $\vec{u}_z^{i(r)}$ is the corresponding unit vector. \vec{u}_\pm^{i0} and \vec{u}_\pm^{r0} are the circular polarization bases for the central wavevector of the incident and reflected beams, respectively. For calculation of the spatial spectra transfer function, we transfer the electric field of each plane wave to the polarization basis for its own wavevector:

$$\begin{pmatrix} \tilde{E}_+^i \\ \tilde{E}_-^i \end{pmatrix} = U_1 \begin{pmatrix} \tilde{E}_+^{i0} \\ \tilde{E}_-^{i0} \\ \tilde{E}_z^{i0} \end{pmatrix}, \tag{S3a}$$

$$\begin{pmatrix} \tilde{E}_+^r \\ \tilde{E}_-^r \end{pmatrix} = U_2 \begin{pmatrix} \tilde{E}_+^{r0} \\ \tilde{E}_-^{r0} \\ \tilde{E}_z^{r0} \end{pmatrix}. \tag{S3b}$$

The matrices U_1 and U_2 are originated from the rotations of coordinates, describing the transformation between the circular polarization basis for the central wavevector and that for each other wavevector:

$$U_1 = \begin{pmatrix} (\vec{u}_+^i)^* \cdot \vec{u}_+^{i0} & (\vec{u}_+^i)^* \cdot \vec{u}_-^{i0} & (\vec{u}_+^i)^* \cdot \vec{u}_z^{i0} \\ (\vec{u}_-^i)^* \cdot \vec{u}_+^{i0} & (\vec{u}_-^i)^* \cdot \vec{u}_-^{i0} & (\vec{u}_-^i)^* \cdot \vec{u}_z^{i0} \end{pmatrix}, \tag{S4a}$$

$$U_2 = \begin{pmatrix} (\vec{u}_+^r)^* \cdot \vec{u}_+^{r0} & (\vec{u}_+^r)^* \cdot \vec{u}_-^{r0} & (\vec{u}_+^r)^* \cdot \vec{u}_z^{r0} \\ (\vec{u}_-^r)^* \cdot \vec{u}_+^{r0} & (\vec{u}_-^r)^* \cdot \vec{u}_-^{r0} & (\vec{u}_-^r)^* \cdot \vec{u}_z^{r0} \end{pmatrix}. \tag{S4b}$$

Due to the continuous condition of the tangential wavevector along the interface, the incident plane wave with the transverse component (k_x, k_y) only generates the reflected plane wave with the same (k_x, k_y) . Therefore, for each incident plane wave with wavevector \vec{k} , the Fourier spectra of the reflected plane wave is

$$\begin{pmatrix} \tilde{E}_+^{r0} \\ \tilde{E}_-^{r0} \\ \tilde{E}_z^{r0} \end{pmatrix} = R \begin{pmatrix} \tilde{E}_+^{i0} \\ \tilde{E}_-^{i0} \\ \tilde{E}_z^{i0} \end{pmatrix} = U_2^\dagger \tilde{R} U_1 \begin{pmatrix} \tilde{E}_+^{i0} \\ \tilde{E}_-^{i0} \\ \tilde{E}_z^{i0} \end{pmatrix}. \quad (\text{S5})$$

Here, matrix R describes the reflection coefficients for left- and right-handed circularly polarized plane waves:

$$\tilde{R} = \frac{1}{2} \begin{pmatrix} r_p + r_s & r_p - r_s \\ r_p - r_s & r_p + r_s \end{pmatrix}, \quad (\text{S6})$$

where r_p and r_s are the Fresnel's reflection coefficients for each p- and s-polarized plane waves with the wavevector \vec{k} , respectively.

Under the paraxial approximation where both the incident and reflected field dominate in the transversal component and $\tilde{E}_z^{i0(r0)} \approx 0$, the dimensions of matrices R , U_1 and U_2 can be reduced to 2×2 . Specifically, the transfer matrices U_1 and U_2 can be approximately evaluated through the geometric phases for left- and right-handed circularly polarized waves as

$$U_j = \begin{pmatrix} \exp(i\Phi_B^j) & 0 \\ 0 & \exp(-i\Phi_B^j) \end{pmatrix}, \quad (\text{S7})$$

where $j = 1, 2$. $\Phi_B^1 = \frac{k_y}{k_0} \cot \theta_0$ and $\Phi_B^2 = -\frac{k_y}{k_0} \cot \theta_0$ are the geometric phases during the

wavevector rotation, while θ_0 is the incident angle of the plane wave component with the central wavevector. Equation (S7) shows that the left- and right-handed circularly polarized light with a wavevector \vec{k} experience the opposite geometric phases during the light reflection.

As shown in Fig. 1 of the main text, the vectorial electric field after the first polarizer P1 can be written as $\vec{E}_i = S_{in}(x, y) \vec{V}_1$, where $S_{in}(x, y)$ is the incident field distribution and $\vec{V}_1 = \frac{i}{\sqrt{2}}(-e^{i\gamma_1}, e^{-i\gamma_1}, 0)^T$ is the unit vector determined by the orientation of P1 under the circular polarization basis of the central wavevector. Then after the reflection on an air-glass interface and analyzed by the second polarizer P2, the measured field distribution is $S_{out}(x, y) = \vec{V}_2^\dagger \cdot \vec{E}_r$ where $\vec{V}_2 = \frac{i}{\sqrt{2}}(-e^{i\gamma_2}, e^{-i\gamma_2}, 0)^T$. By a spatial Fourier transform, $S_{in(out)}$ can also be written as the superposition of plane waves as $S_{in(out)} = \iint \tilde{S}_{in(out)}(k_x, k_y) \exp(ik_x x) \exp(ik_y y) dk_x dk_y$. Thus, we have

$$\begin{pmatrix} \tilde{E}_+^{i0} \\ \tilde{E}_-^{i0} \\ \tilde{E}_z^{i0} \end{pmatrix} = \tilde{S}_{in}(x, y) \vec{V}_1, \quad (\text{S8a})$$

$$\tilde{S}_{out}(x, y) = \vec{V}_2^\dagger \cdot \begin{pmatrix} \tilde{E}_+^{r0} \\ \tilde{E}_-^{r0} \\ \tilde{E}_z^{r0} \end{pmatrix}. \quad (\text{S8b})$$

By substituting Eq. (S8a) and (S8b), Eq. (S5) becomes

$$\vec{V}_2 \tilde{S}_{out}(k_x, k_y) = R \vec{V}_1 \tilde{S}_{in}(k_x, k_y). \quad (\text{S9})$$

According to Eq. (S9), the spatial spectral transfer function between the specimen's distribution

and the finally measured one is

$$H \equiv \frac{\tilde{S}_{out}(k_x, k_y)}{\tilde{S}_{in}(k_x, k_y)} = \vec{V}_2^\dagger R \vec{V}_1. \quad (\text{S10})$$

By calculation, the spatial spectral transfer function H in Eq. (S10) is

$$H = r_p \sin \gamma_1 \sin \gamma_2 + r_s \cos \gamma_1 \cos \gamma_2 + \frac{\delta (r_p + r_s) \sin (\gamma_2 - \gamma_1)}{2} k_y, \quad (\text{S11})$$

where $\delta = \frac{2}{k_0} \cot \theta_0$ corresponds to the transverse shift for the circularly polarized plane waves.

We note that the two items in Eq. (S11) exactly correspond to the Malus's Law in the configuration of Fig. 1, while the third item is due to the Imbert-Fedorov (IF) shift.

2 Experimental measurement of spatial spectral transfer function

We experimentally measure the spatial spectral transfer functions of different directional spatial differentiations under the cross-polarization condition. Specifically, we measure the incident and reflected spatial spectra, and the spatial spectral transfer functions are obtained by normalizing the reflected spectrum data with the incident ones. The experiment setups for measuring the spatial spectral transfer functions is schematically shown in Fig. S1. A green laser is collimated to a Gaussian beam. Then we use a lens L1 to focus the incident beam to amplify the amplitudes of the plane wave components with higher spatial frequencies, which is advantageous for the measurement of spatial spectral transfer function with a relatively broad spatial bandwidth. The beam is subsequently polarized by a polarizer P1 with an orientation angle γ_1 as shown in Fig. S1(a) and focuses on a dielectric interface. e.g. an air-glass interface in our experiment. After reflected on the air-glass interface, the beam is analyzed by another polarizer P2 whose orientation angle is

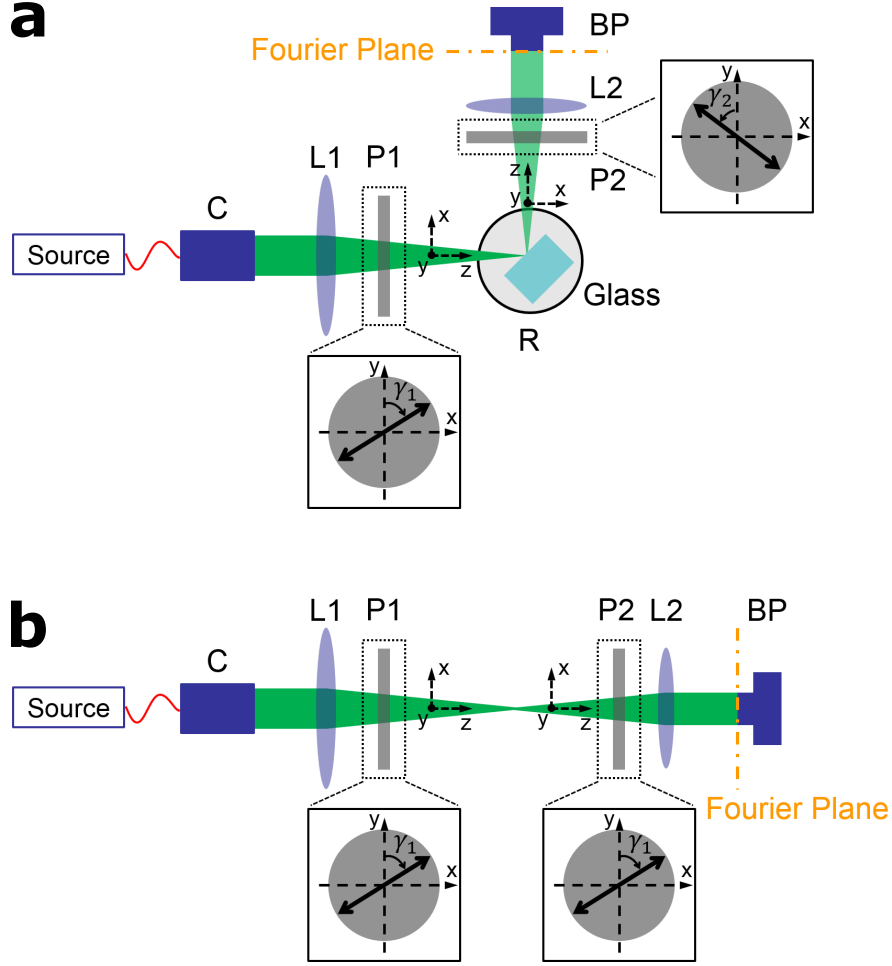


Fig S1 Experimental setup for measuring the spatial spectral transfer function. (a) Experimental setup for measuring the reflected spatial spectrum: collimator C; lenses L1 and L2 with focal lengths 50mm and 30mm , respectively; polarizers P1 and P2; glass slab (material BK7); precision rotator R; and beam profiler BP (Ophir SP620U). A green laser (wavelength $\lambda_0 = 532\text{nm}$) is connected to the collimator through a fiber with a polarization controller. (b) The experimental setup for measuring the incident spatial spectrum, in which the polarizer P2 is oriented with the same angle of P1.

γ_2 , determined by the cross-polarization condition. Another lens L2 performs Fourier transform of the reflected field and the corresponding reflected spatial spectra is measured by a beam profiler (Ophir SP620U) at the back focal plane of L2. On the other hand, the incident spatial spectra are obtained by removing the glass and rotating the reflection path (lens L2 and polarizer P2) as shown in Fig. S1(b), while the orientation angles of P2 are rotated to be the same as those of P1. We note that the two polarizers are placed between lenses L1 and L2 in order to avoid the polarization ro-

tation induced by the geometric phase during light focusing and collimating.¹ By normalizing the reflected spectrum data with the incident ones, we can obtain the spatial spectral transfer functions of the adjustable spatial differentiation.

3 Experimental measurement of the differentiation direction angle φ and the proportionality coefficient A for different combination of γ_1 and γ_2

To verify the theoretical result of Eq. (3) in the main text, here we show the experimental measurement of the differentiation direction angle φ and the proportionality coefficient A for different combinations of γ_1 and γ_2 . Experimentally, we acquire the direction angles and proportionality coefficients by measuring the spatial spectral transfer functions (Fig. S1). Their gradient directions show the directions of spatial differentiation while gradient values indicate the proportionality coefficients. Specifically, we obtain the values of C_1 and C_2 , by fitting the horizontal and vertical gradients of the measured spatial spectral transfer functions, respectively. Then we calculate the direction angles and proportionality coefficients based on the obtained values of C_1 and C_2 .

As shown in Fig. S2, it corresponds to a measured spatial spectral transfer function with $\gamma_1 = 18.0^\circ$ and $\gamma_2 = 84.23^\circ$, which satisfies the cross-polarization condition. We extract the data on $k_x = 0$ and $k_y = 0$ [the red dashed lines in Fig. S2(a)] and obtain the values of C_1 and C_2 by fitting their slopes, respectively. In Figs. S2(b) and S2(c), the data exhibit linear dependences on k_x and k_y , respectively, and the fitting results are $|C_1| = 0.1423$ and $|C_2| = 0.1964$. With $\varphi \in [0, 180]$ and Fig. S2(a) showing a rough gradient direction, we have $C_1 = -0.1423$ and $C_2 = -0.1964$, respectively. According to the theoretical spatial spectral transfer function in Eq. (3) in the main text, the direction and proportionality coefficient of the spatial differentiation are $\vec{l} = (C_1, C_2)$ and $A = |\vec{l}| = \sqrt{(C_1)^2 + (C_2)^2}$, respectively. Therefore, in the case of Fig. S2(a), we have

$\varphi = 144.08^\circ$ and $A = 0.2425$.

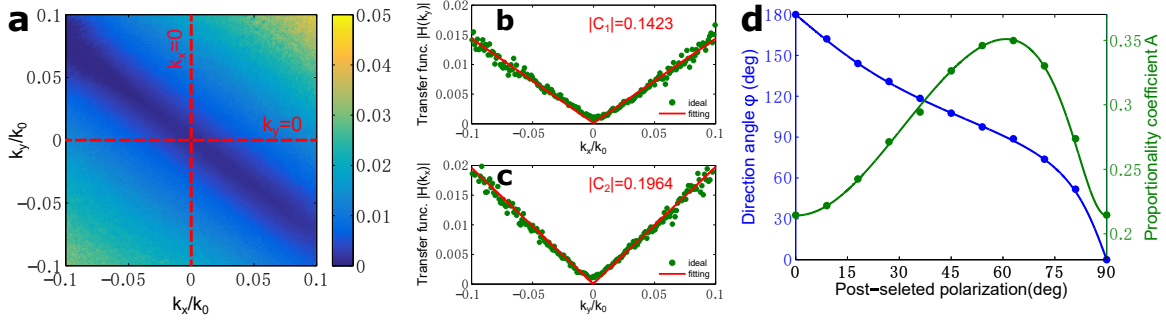


Fig S2 Experimental measurement of direction angle φ and the proportional coefficient A . In these results, the incident angle of the beam is $\theta_0 = 45^\circ$ and a BK7 glass slab works as the reflector with refractive index 1.5195 at the wavelength $\lambda_0 = 532\text{nm}$. (a) Experimentally measured spatial spectral transfer function with $\gamma_1 = 18.0^\circ$ and $\gamma_2 = 84.23^\circ$. (b, c) Fitting results of the data on $k_x = 0$ and $k_y = 0$ [red dashed lines in (a)], respectively. (d) Values of φ (blue) and A (green) under different combinations of γ_1 and γ_2 . The solid and dotted lines are the theoretical and experimental results, respectively.

Following the above method, we experimentally measure the results under different combinations of γ_1 and γ_2 , among which four specific cases ($\varphi = 45^\circ, 90^\circ, 135^\circ$ and 180°) are shown in the main text. The experimental results are plotted as the dotted lines in Fig. S2(d) and coincide well with the theoretical results, which are calculated from Eq. (3) and shown as the solid lines. The results again exhibit the adjustability of the proposed spatial differentiation. These coefficients are quantitatively important. For instance, differentiated results along different directions should be first normalized by their corresponding proportionality coefficients before being utilized with each other in the meantime.

4 Field transformation in the bias introduction scheme

In the biased condition $r_{p0} \sin \gamma_1 \sin \gamma_2 = -r_{s0} \cos \gamma_1 \cos \gamma_2 + b$, the spatial spectral transfer function Eq. (S11) becomes

$$H = -(C_1 k_x + C_2 k_y) + b. \quad (\text{S12})$$

In the spatial domain, the measured field distribution is

$$S_{out}(x, y) = i \left(C_1 \frac{\partial S_{in}}{\partial x} + C_2 \frac{\partial S_{in}}{\partial y} \right) + b S_{in} = iA \frac{\partial S_{in}}{\partial l} + b S_{in}. \quad (\text{S13})$$

For an observed field with a phase distribution $\psi(x, y)$, the incident field is $S_{in} = e^{-i\psi(x,y)}$. According to Eq. (S13), we have the output field written as

$$S_{out}(x, y) = A \frac{\partial \psi}{\partial l} e^{-i\psi(x,y)} + b e^{-i\psi(x,y)} = \left(A \frac{\partial \psi}{\partial l} + b \right) e^{-i\psi(x,y)}. \quad (\text{S14})$$

By direct intensity detection, the result is measured as the absolute value $\left| A \frac{\partial \psi}{\partial l} + b \right|$. As a consequence, with an appropriate positive bias b , the measured distribution appears brighter or darker at areas with positive or negative directional derivative $\partial \psi / \partial l$, respectively.

5 Specific orientation angles of polarizers P1 and P2 for different directional spatial differentiations and biased images

The orientation angles γ_1 and γ_2 for a certain direction angle φ can be determined according to Eq. (2). Figure 2(b) in the main text plots the values of γ_1 and γ_2 under every φ for a specific case, in which the wavelength of laser source is $\lambda = 532nm$ and the corresponding refractive index of the BK7 glass is 1.5195. For examples, the values of γ_1 and γ_2 for the direction angles $\varphi = 45^\circ, 90^\circ, 135^\circ$ and 180° are listed in Table S1. In these cases, the cross-polarization condition

Table S1 Orientation angles γ_1 and γ_2 of polarizers for spatial differentiation with different direction angle φ , and the corresponding bias values

	Figure 3(a)	Figure 3(b)	Figure 3(c)	Figure 3(d)
φ	45°	90°	135°	180°
γ_1	82.25°	60.86°	23.65°	0°
γ_2	23.65°	60.86°	82.25°	90°
b	0	0	0	0

Table S2 Orientation angles γ_1 and γ_2 of polarizers for biased differential contrast images with different bias values b

	Figure 4(a)	Figure 4(b)	Figure 4(c)	Figure 4(d)
φ	45°	90°	135°	180°
γ_1	82.25°	60.86°	23.65°	0°
γ_2	32.65°	65.86°	84.25°	91°
b	0.0163	0.0151	0.0100	0.0054

is critically satisfied so that the corresponding bias values are $b = 0$.

The biased differential contrast images can be obtained just by controlling the value of γ_2 deviating from the cross-polarization condition. For example, we show biased images with different bias values in the main text [Figs. 4(d-g)]. We keep the values of orientation angle the same as in Table S1 and rotate polarizer P2 for deviation angles 9°, 5°, 2° and 1°, respectively. The new values of γ_2 and the corresponding bias values b are listed in the Table S2. These four cases correspond to biased differential contrast images Figs. 4(d-g) in the main text.

6 Acquisition of directional derivatives of the phase distribution

To acquire the directional derivatives of a phase distribution, we first experimentally measure the non-biased differential contrast images with $b = 0$. For example, Figs. S3(a, b) exhibit non-biased differential contrast images of the phase distribution [Fig. 4(b) in the main text] with direction angles $\varphi = 180^\circ$ and $\varphi = 90^\circ$, respectively. We then introduce a positive and very small bias as a perturbation, by rotating the polarizer P2 to slightly increase the value of γ_2 . The resulted images are measured as Figs. S3(c, d). Consequently, as we subtract Figs. S3(a, b) from Figs. S3(c, d), the signs of their difference values indicate the signs of the directional derivatives [Figs. S3(e, f)], respectively.

Combining the obtained sign [Figs. S3(e, f)] of $\partial\psi/\partial l$ and the absolute values calculated from Figs. S3(a, b), we can experimentally acquire the first-order directional derivatives of $\psi(x, y)$.

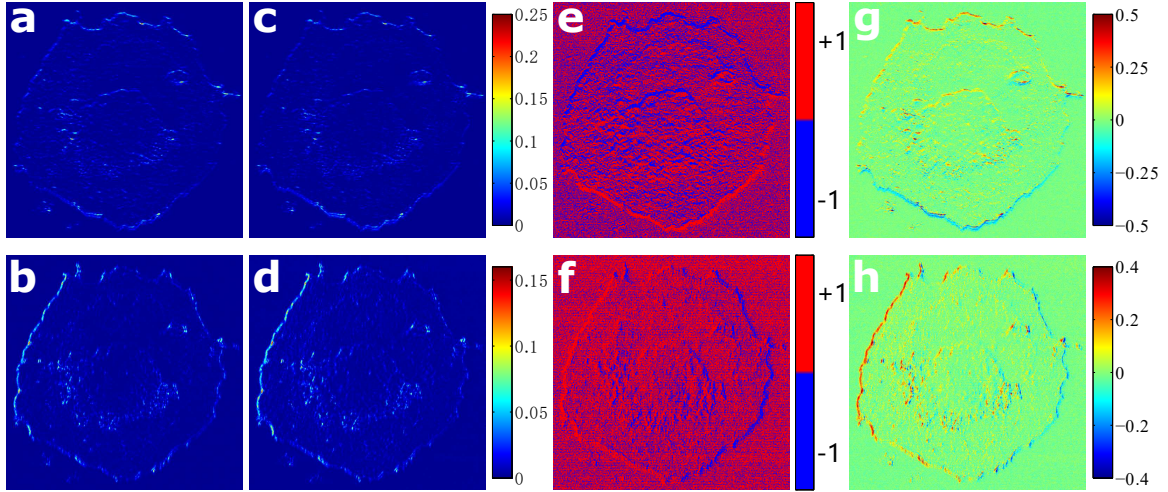


Fig S3 Experimental acquisition of directional derivatives of the phase distribution. (a, b) Non-biased differential contrast images with direction angles $\varphi = 180^\circ$ and $\varphi = 90^\circ$, respectively. (c, d) Biased differential contrast images with a positive and very small bias as a perturbation on the basis of (a) and (b), respectively. (e, f) Signs of the vertical and horizontal partial derivatives, respectively, consisting of the values of +1 and -1. (g, h) Acquired vertical and horizontal partial derivatives, respectively.

Figures S3(g, h) show the obtained vertical and horizontal partial derivatives of phase distribution Fig. 4(b), respectively, which are the results shown as Figs. 5(a, b) in the main text.